ChemPubSoc Europe

DOI: 10.1002/slct.201902216

Chemistry SELECT Full Papers

Electro, Physical & Theoretical Chemistry

Modelling Vibrational Dissociation of $[H_2–HCO]^+$

Peter Kraus,* H. Tobias Alznauer, and Irmgard Frank[a]

The $[H_2–HCO]^+$ complex is likely to be one of the most important complexes in interstellar space, as it is a complex of the most abundant interstellar species. In the current work, we investigate the interaction energy and potential surface of the complex using a range of computational methods. The dynamics of the complex are investigated by incorporating an external time-dependent field into Car-Parrinello molecular dynamics (CPMD) and inducing a vibrationally activated dissociation. This excitation method is compared to a normal-mode excitation from the equilibrium structure. The results agree well with the available experimental data: an excitation to the first vibrationally-excited state of either of the high-frequency HCO^+ modes (ν_2, ν_3) causes a dissociation of the complex on picosecond timescales.

1. Introduction

Since the advent of radio-millimeter telescopes in the 1970's, experimental observations of dense clouds led to the discovery of many poly-atomic species in the interstellar medium.[1] While the reaction conditions in space are significantly different from the Earth's atmosphere, the detection of radical[2] and later ionic species,[3] coupled to the interesting non-equilibrium chemistry of interstellar clouds, may have important implications for gas-phase kinetic models used in combustion science[1] or climate change research.[4]

Here we focus on the van der Waals complex of some of the most-abundant species in the interstellar medium: $[H_2–HCO]^+$. The most-abundant species in space, H_2, is thought to be approximately 10 000 × more abundant than the second most-abundant CO.[1] The formyl cation (HCO^+) has been first observed in dense clouds by Herbst and Klemperer,[3] and has been instrumental in estimating the abundance of CO.[5] A complex of these species is therefore a logical starting point for the investigation of reaction dynamics in interstellar media.

The $[H_2–HCO]^+$ complex can be prepared experimentally in a radiative association process[6] at 90 K.[7,8] However, the H_2 in the complex is quickly displaced by another CO molecule to form the $[OC-HCO]^+$ species.[7,9] The $[H_2–HCO]^+$ system has been investigated using infrared spectroscopy and the vibrational pre-dissociation spectra were obtained by Bieske et al.[10] The depopulation of vibrationally excited states is rapid: depending on the excited vibrational mode, the dissociation occurs on a picosecond timescale.[10] The $[D_2–DCO]^+$ complex has also been studied experimentally.[11] The most recent investigation of the $[H_2–HCO]^+$ complex is the theoretical study by Massó and Wiesenfeld,[12] who reported a detailed potential energy surface (PES) of interaction energies (E_{int}) using a counterpoise-corrected coupled cluster method including full triples, with basis set extrapolated to the complete basis set limit (CP–CCSDT/CBS).

While the dynamics of the $[H_2–HCO]^+$ complex have been investigated experimentally, a computational study of the dissociation dynamics has, to our knowledge, not been carried out. The comparably simple electronic structure of the cation, containing just 12 valence electrons, makes the dynamical timescales of the system computationally tractable with ab initio methods. The full potential energy surface of the $[H_2–HCO]^+$ complex is 9-dimensional. A significant progress has been achieved in quantum dynamical calculations of related systems, for example using 6-dimensional potential to model H_2 collision with CO,[13] or an 8-dimensional potential energy surface to investigate H-abstraction of CH_4 by exploiting symmetry.[14] However, performing a full dimensional quantum dynamics investigation of the $[H_2–HCO]^+$ system is currently prohibitively expensive, as a potential energy surface (PES) suitable for such purpose has not yet been published. Therefore, in the current work, we investigate the dynamics of vibrationally activated dissociation of the complex using ab initio molecular dynamics (AIMD) and density functional theory (DFT). First, the uncertainty due to the density functional approximation (DFA) is estimated by a comparison to symmetry adapted perturbation theory (SAPT) as well as wavefunction theory (WFT) calculations performed on the system, and to the most relevant regions of the high-accuracy CP-CCSDT/CBS potential surface of Massó and Wiesenfeld.[12] The complex is then investigated dynamically, by comparison to experimental spectra, and by a mode-selective vibrational excitation. The latter comparison is performed using both normal-mode excitation, as well as time-dependent external fields. Following an excitation, the dissociation of the vibrationally excited $[H_2–HCO]^+$ and $[D_2–DCO]^+$ is studied. Finally, the influence of quantum tunnelling on the dynamics is assessed using path integral methods on a selected case.

[a] Dr. P. Kraus, Dr. H. T. Alznauer, Prof. Dr. I. Frank
Institut für Physikalische Chemie und Elektrochemie, Leibniz Universität Hannover, Callinstrasse 3 A, 30167 Hannover, Germany
E-mail: peter.kraus@theochem.uni-hannnover.de

Supporting information for this article is available on the WWW under https://doi.org/10.1002/slct.201902216

2. Results and Discussion

An overview of the coordinate system overlaid over the equilibrium geometry of the $[H_2–HCO]^+$ complex obtained with PBE0-D2/MT is shown in Figure 1. For this T-shaped global minimum, the equilibrium monomer separation is r_{COM} = 3.404 Å, and the angle a(O=C···H_2) = 180°. Bieske et al. propose another local minimum in this system:[10] an out-of-plane minimum with a(O=C···H_2) ~ 90° here denoted $[H_2<HCO]^+$. Other stationary points are obtained by a rotation of the H_2 monomer around its own center of mass (denoted [H–H–HCO]$^+$), as well as around the HCO monomer resulting in a structure where the the H_2 monomer is coordinated to the O atom (denoted $[HCO–H_2]^+$).[10] All stationary points on the $[H_2–HCO]^+$ PES are shown in Figure S1 in the Supporting information.

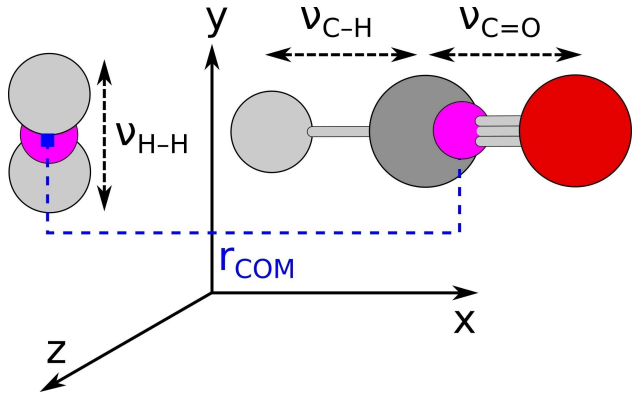

Figure 1. The geometry at the global, T-shaped minimum, obtained with PBE0-D2/MT, is shown along with the coordinate system used throughout the current work. The centres of masses of monomers are shown in pink. The vibrational modes and the intermonomer separation are also indicated.

2.1. Potential surfaces and interaction energies

To estimate the error due to the methods applied in our AIMD calculations, we report zero point corrected interaction energies calculated using a variety of methods, along with literature data in Table 1.

The results of the plane-wave calculations (with a MT basis set) are in a reasonable agreement in both E_{int} and $\triangle E_{ZPE}$ from the Gaussian-orbital calculations. However, both DFAs overbind the complex by up to 10 kJ/mol compared to our CP–MP2/CBS + δ(T) results at the respective minima, and by up to 13 kJ/mol compared to the previous correlated wavefunction theory results.[10,12] For comparison, the E_{int} at the optimised geometry obtained with a state-of-the-art single-hybrid DFA (ωB97M-V[15]) is within 2.5 kJ/mol of the CP-MP2/CBS + δ(T) result. This somewhat large overbinding in the PBE-based DFAs with respect to the true energetics of the system is likely to introduce systematic errors in the dynamics of the system.

Table 1. Calculated and literature interaction energies for the $[H_2–HCO]^+$ system at the global T-shaped minimum, in kJ/mol. Results marked with † obtained with the fixed monomer approximation (see text).

Method Geometry	Energy	E_{int}	$\triangle E_{ZPE}$
PBE0-D2/MT	PBE0-D2/MT	-27.30	5.34
PBE0-D2/AVQZ	CP-PBE0-D2/AVQZ	-26.58	6.49
PBE0-D2/AVQZ	CP-MP2/CBS + δ(T)	-19.22	–
PBE–D2/MT	PBE–D2/MT	-29.10	5.07
PBE–D2/AVQZ	CP-PBE–D2/AVQZ	-30.88	6.18
PBE–D2/AVQZ	CP-MP2/CBS + δ(T)	-20.51	–
ΩB97M–V/AVQZ	CP-ωB97M–V/AVQZ	-20.82	–
QCISD(T)/6-311(2df,2pd)	QCISD(T)/6-311(2df,2pd)[10]	-17.28	7.11
MP2/CBS + δ(T)	CP-MP2/CBS + δ(T)	-18.46	–
†	CP-MP2/CBS + δ(T)	-18.02	–
†	SAPT2 + (CCD)δMP2/AVTZ	-17.74	–
†	CP-CCSDT/CBS[12]	-17.79	–

The PES of Massó and Wiesenfeld[12] is calculated with a fixed monomer approximation, in which the geometry of the H_2 and HCO^+ units is kept fixed at r(H–H) = 0.7666 Å, r(C=O) = 1.1055 Å, and r(C-H) = 1.0919 Å. When we apply these constraints (denoted by † in Table 1), the partially-relaxed geometries calculated with SAPT2 + (CCD)δMP2/AVTZ and CP-MP2/CBS + δ(T) are within 0.3 kJ/mol in E_{int} and 0.001 Å in r_{COM} of the reported CP-CCSDT/CBS data. From comparison with the fully-relaxed results, the fixed monomer approximation introduces an error of ~ 0.45 kJ/mol in E_{int}. These small energy differences are unlikely to be responsible for the difference in the stationary points on the reported $[H_2–HCO]^+$ PESs.[10,12]

The effect of monomer separation on the interaction energy of the complex with the fixed monomer approximation applied is shown in Figure 2. The interaction energy obtained with all methods converges to the same value at approximately 5 Å, but does not vanish until separations larger than 6 Å. As

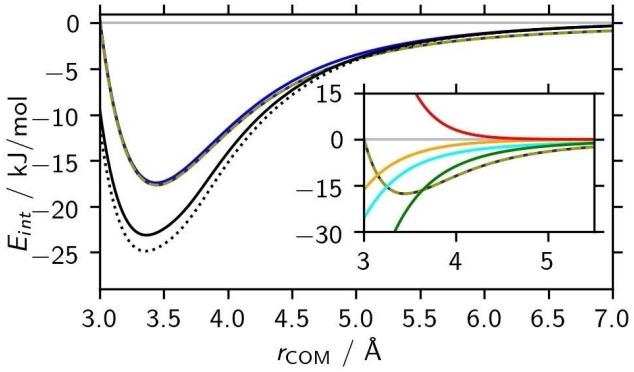

Figure 2. Interaction energies of the $[H_2–HCO]^+$ complex as a function of monomer distance. Results obtained with SAPT2 + (CCD)δMP2/AVTZ (gray dashed), MP2/CBS + δ(T) (blue), PBE0-D2/AVQZ (black) and PBE–D2/AVQZ (black dotted). The SAPT terms arising from exchange (red), induction (green), electrostatics (cyan) and dispersion (orange) are included in the inset.

already shown in Table 1, the PBE–D2/AVQZ and PBE0-D2/AVQZ methods overestimate the interaction energies at intermediate separations, achieving only a qualitative agreement with the wavefunction methods. At close ranges (< 3.0 Å), the SAPT analysis (inset) shows the interaction is dominated by repulsive exchange (red). The largest attractive contribution at intermediate distances is from induction contributions (green), as can be expected for an interaction of a charged ion with a neutral species. However, the electrostatic (cyan) and dispersion (orange) contributions are not negligible, and contribute significantly to the binding energy.

The barrier to the internal rotation of the H_2 monomer within the plane of the molecule, i.e.

$$\Delta E^{\neq} = E([H-H-HCO]^+) - E([H_2-HCO]^+),$$

is shown along with the interaction energy at the transition state in Table 2. The PBE–D2 and PBE0-D2 methods significantly overpredict the interaction energy as well as the barrier height. A potential energy surface of the region between the minimum and the transition state obtained with the fixed monomer approximation is shown in Figure 3. The agreement between the two density functionals is good. When compared to the correlated WFT potential energy surface, the DFA surface is much deeper, and the energy penalty for H_2···HCO angles other than 90° is smaller.

Table 2. Calculated and literature interaction and activation energies for the transition state $[H–H–HCO]^+$, in kJ/mol.

Method Geometry	Energy	E_{int}	$\triangle E^{\neq}$
PBE0-D2/AVQZ	CP-PBE0-D2/AVQZ	-7.34	19.15
PBE–D2/AVQZ	CP-PBE–D2/AVQZ	-11.80	19.08
MP2/CBS + δ(T)	CP-MP2/CBS + δ(T)	-3.06	13.92
QCISD(T)/6-311(2df,2pd)	QCISD(T)/6-311(2df,2pd)[10]	-3.36	15.40
†	CP-CCSDT/CBS[12]	-3.57	14.22

The results of our calculations for the second in-plane transition state, $[HCO–H_2]^+$, are shown in Table 3. In the DFA potential surfaces, this stationary point is bound much more weakly than the linear $[H–H–HCO]^+$ transition state discussed above. With WFT, the two transition states are energetically much closer together. The calculated geometry of this weakly bound state also varies considerably, with the density functionals predicting a separation around 0.1 Å shorter. A SAPT analysis shows the binding is of a mixed character, with electrostatics, induction and dispersion effects contributing equally towards the E_{int}. This is in contrast with the global minimum, where the stabilisation due to induction is significantly stronger than the electrostatic or dispersion interaction.

Table 3. Calculated and literature interaction and activation energies, as well as monomer distances for the transition state $[HCO–H_2]^+$, in kJ/mol and Å.

Method Geometry	Energy	E_{int}	$\triangle E^{\neq}$	r_{COM}
PBE0-D2/AVQZ	CP-PBE0-D2/AVQZ	-3.08	21.57	3.480
PBE–D2/AVQZ	CP-PBE–D2/AVQZ	-3.60	24.37	3.458
MP2/CBS + δ(T)	CP-MP2/CBS + δ(T)	-2.82	14.94	3.541
QCISD(T)/6-311(2df,2pd)	QCISD(T)/6-311(2df,2pd)[10]	-1.74	15.53	3.538
†	CP-CCSDT/CBS[12]	-2.97	14.82	3.625

Finally, the out-of-plane stationary point $[H_2 < HCO]^+$ has been located using both DFA's, as well as the MP2/CBS + δ(T) calculations (see Table 4 for energies). The interaction energy obtained with the latter is comparable to the QCISD(T) data of

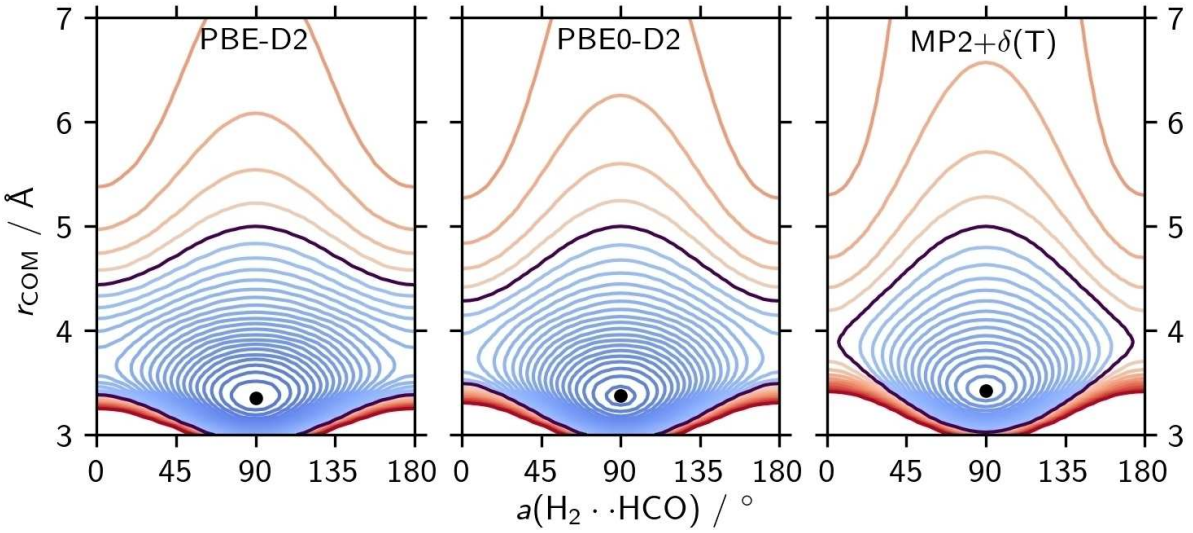

Figure 3. Potential energy surfaces between the $[H_2–HCO]^+$ and $[H–H–HCO]^+$ conformations with PBE–D2, PBE0-D2 and MP2 + δ(T). Contour spacing is 1 kJ/mol, with the black contour at r_{COM} = 5.0 Å, a(H_2···HCO) = 90° point taken as the reference point. Blue contours are negative, red are positive.

Table 4. Calculated and literature interaction energies and zero point energy differences for the local minimum $[H_2 < HCO]^+$, in kJ/mol.

Method Geometry	Energy	E_{int}	$\triangle E_{ZPE}$
PBE0-D2/AVQZ	CP-PBE0-D2/AVQZ	-15.79	6.14
PBE–D2/AVQZ	CP-PBE–D2/AVQZ	-19.65	6.02
MP2/CBS + δ(T)	CP-MP2/CBS + δ(T)	-10.87	–
QCISD(T)/6-311(2df,2pd)	QCISD(T)/6-311(2df,2pd)[10]	-8.67	–

Bieske et al.[10] This contrasts with the later study of Massó and Wiesenfeld, where no such stationary point was found.[12]

Both of the DFAs are able to qualitatively model the main features of the $[H_2–HCO]^+$ system. Quantitatively, both methods overbind the complex significantly when compared to the highly-accurate MP2/CBS + δ(T) calculations. At 80 K, a slow-down by a factor of 10^{-4} in the internal rotation of H_2 and 10^{-6} for a complete dissociation of the complex can be expected due to the difference in the barrier heights.

2.2. Vibrational modes of unperturbed $[H^2–HCO]^+$

To further validate the chosen methods by considering dynamical parameters, rather than just stationary energy points, we compare the frequencies of the vibrational modes of the complex obtained analytically, as well as frequencies from the AIMD trajectories which should contain anharmonic effects, to the frequencies obtained experimentally by Bieske et al.[10] The power spectra are calculated from the 5 ps long equilibration trajectories (NVE, started at ~ 90 K) with TRAVIS.[16] The results are shown in Figure 4. The agreement with experiment

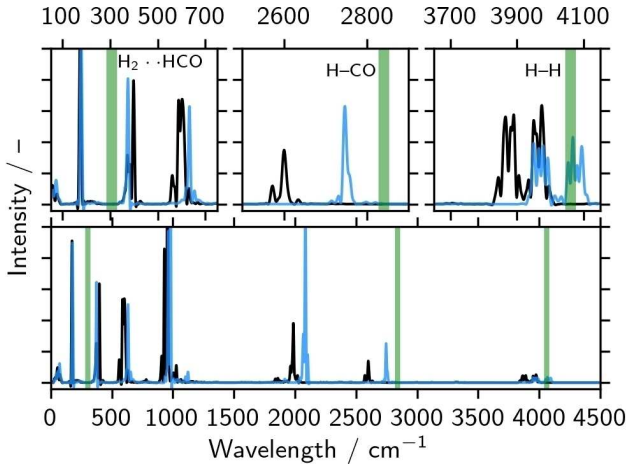

Figure 4. Normalised power spectra of $[H_2–HCO]^+$ equilibrated at 80 K, calculated with PBE–D2 (black) and PBE0-D2 (blue) and with $m_e = 500$ a.u., compared to experimental data (green).[10]

for the H–H and H_2···HCO modes is acceptable for both density functionals, while in the H–CO mode a significant underprediction by the PBE–D2 functional is observed.

However, spectra obtained from Car-Parrinello calculations are known to suffer from a red shift due to the orbital inertia caused by the artificially increased electronic mass.[17] We have corrected for this effect by extrapolation towards a mass of 1 m_e (from 500 m_e and 300 m_e calculations, accompanied by an appropriate reduction in timestep). The extrapolated results are shown in Table 5 in addition to the experimental results of

Table 5. Experimental[10] and PBE0-D2/MT frequencies for the vibrational modes of $[H_2–HCO]^+$, in cm^{-1}.

ν	Mode	Frequencies / cm^{-1} Exp.[10]	Harmonic	AIMD xtpl.	AIMD raw
ν_1	H—H	4060	4222	4218	4024
ν_2	H—CO	2840	2824	2815	2747
ν_4	H_2···HCO	300 - 305	406	366	374
ν_3	HC=O	–	2137	2045	2085
$\nu_{5,7}$	HCO bend	–	987, 1016	961, 1088	963, 980
$\nu_{6,9}$	Low freq. bend	36 - 39	190, 206	176	178
ν_8	H_2 rock	–	663	637	633

Bieske et al.,[10] the harmonic frequencies obtained with PBE0-D2/MT, and the "raw" AIMD frequencies from the 500 m_e calculation shown in Figure 4.

For the H–H mode (ν_1), the "raw" AIMD frequency is in an excellent agreement (within 1%) of the experimental value. However, upon correction for the effect of the electronic mass, the agreement worsens (to within 4%). The harmonic wavenumber is essentially the same as this corrected AIMD result. The behaviour is similar in isolated H_2: the PBE0-D2/MT harmonic frequency (4355 cm^{-1}) is significantly higher than the experimental wavenumber (4161 cm^{-1});[18] while the AIMD results are 4128 cm^{-1} with 500 m_e and 4343 cm^{-1} after extrapolation. The effective increase in hydrogen mass from $m_H = 1837$ m_e to 2337 m_e leads to error cancellation. Similar effects can be seen in the H–CO (ν_2) mode, where the difference between the harmonic and corrected AIMD results is negligible. For the lower frequency modes, the AIMD values show a more significant anharmonicity. This discrepancy of AIMD-based spectra from the anharmonic experimental values at high frequencies has been reported previously: the spectrum of liquid water is underestimated above 2000 cm^{-1},[19] while the high-frequency modes in methanol and pinacol are overestimated.[20] This high-frequency effect has been attributed to the error of the DFA rather than an inadequacy of AIMD,[20] which leads us to believe that the shape of the H–H potential with the PBE0-D2 functional is incorrect.

The experimental frequency of the H_2···HCO intermolecular stretch (ν_4) can be determined from a combination band with ν_2, supported by an analysis of centrifugal distortion constants.[10] The analytic harmonic frequency overestimates this experimental result by ~ 30%. For this mode, the anharmonic behaviour in the AIMD improves the agreement to within 20%. The anharmonicity of the PBE0-D2/MT potential (40 cm^{-1}) is in line with the 33 cm^{-1} anharmonicity reported by Bieske et al.[10] Furthermore, the calculated AIMD power spectra also contain a small-intensity band at around 3110 cm^{-1}. If we

assume this is the $\nu_2 + \nu_4$ combination band, we arrive at a "raw" AIMD frequency of 378 cm^{-1}, which is in a good agreement with the actual mode at 374 cm^{-1}: the calculations thus support the assignment of Bieske et al.[10] despite the somewhat large disagreement in the frequency.

The experimental frequencies attributed to the ν_6 and ν_9 bending modes can also be determined from combination bands.[10] The anharmonicity of the bands is significant, as shown by our AIMD results. Unfortunately, the baseline of the power spectrum in the immediate vicinity of the ν_2 peak is rather noisy, which prevents further assignment.

2.3. Dynamics of vibrationally excited $[H_2–HCO]^+$

Bieske et al. observed broadening of the rotational lines in vibrationally excited $[H_2–HCO]^+$, and concluded that its dissociation is extremely rapid, occurring at a picosecond timescale for species in the first excited state of the ν_2 mode (H–CO stretch).[10] When the ν_1 mode (H–H stretch) was excited, a 250 ps value was proposed as a lower limit to the lifetime of the complex.[11] The dissociation is therefore "decidedly nonstatistical"[10] as the ν_1 mode is ~1000 cm^{-1} higher in energy than the ν_2 mode, but its dissociation rate is significantly slower.

It is worth noting, that while the E_{int} obtained with PBE0-D2 is 27.30 kJ/mol, the zero point effects in the complex lower this barrier to 20.66 kJ/mol. This value lies well below the first vibrational excitation of both H–CO and HC=O stretches (with PBE0-D2: $\nu_2 = 33$ kJ/mol; $\nu_3 = 25$ kJ/mol).

The results for this system, obtained with an excitation using external fields, are shown in Figure 5. As the nuclear dynamics in AIMD calculations are classical, the system is not necessarily constrained to quantized vibrational or rotational levels. As a consequence, it is possible to deposit arbitrary amounts of energy from the external field into the system (see Supporting information for details). To facilitate the discussion, we have chosen to normalise the deposited energy as an "equivalent vibrational level" (EVL), here defined as the energy uptake normalised by the frequency of the excited bond. The energy uptake from the external field is shown in Figure S1, with the Kohn-Sham energy at the equilibrium geometry as the reference point. For the frequency of the excited bond, appropriate ν_2 or ν_3 are used. Between 2 and 16 calculations were carried out at each EVL, with the positions of the atoms randomised by < 0.01 Å. The trajectories were followed for up to 500 ps (100 ps for PBE0-D2) corresponding to ~4 million timesteps, or until a dissociation event occurred. The latter has been evaluated against a dissociation criterium of $r_{COM} >= 5.0$ Å. While at this separation the intermonomer interaction is still non-zero, we believe our choice is justified, as due to the imposed periodic boundary conditions and the use of plane-wave basis sets a larger domain would incur a significantly increased computational cost.

As expected, the dissociation rate correlates with the overall energy uptake (R^2 of 0.767), shown in the top panel of Figure 5. However, when the data is plotted against EVL and split based on the excited vibrational modes, a considerably better

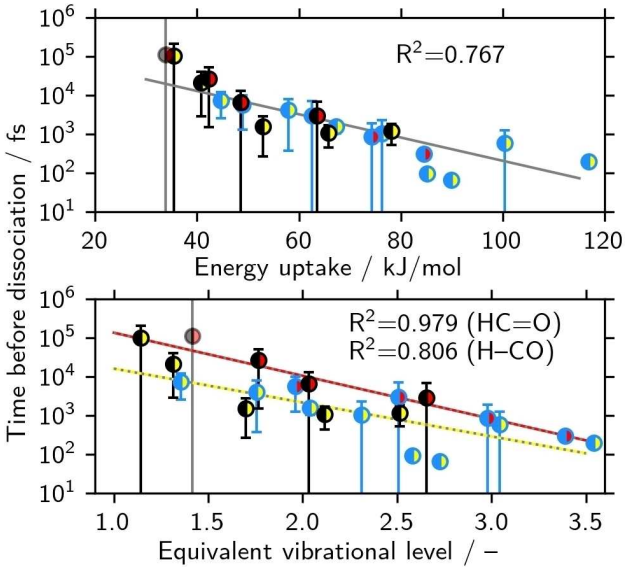

Figure 5. Time before dissociation for vibrationally excited $[H_2–HCO]^+$ plotted as a function of EVL and energy uptake. Results obtained with PBE0-D2 (blue) and PBE–D2 (black) for C–H excitation (yellow shading) and C=O excitation (red shading). The gray, red, and yellow lines are linear regressions to all data, HC=O excitation, and H–CO excitation data, respectively. Error bars correspond to three standard errors ($3\times\sigma/\sqrt{n}$, with n between 2 and 16). In the lowest energy HC=O excitation (grey shading), dissociation occurred within 500 ps in only in 7 out of 8 of cases

correlation is obtained, especially for the HC=O excitation. With the exception of one trajectory, all calculations performed at EVLs above 1.0 show dissociation on picosecond timescales. The calculations carried out at lower EVLs (not shown) did not lead to a dissociation of the complex within 500 ps. The calculations investigating H–CO excitation at EVL ~ 2.7 dissociate very quickly, with a very small standard error between the four runs, with the dissociation at EVLs > 3.0 proceeding slower again. This is partially attributed to the rather low statistical strength of the dataset, as all excited trajectories are generated from the same equilibrated state: the fast dissociation at these intermediate excitations might be fortuitous.

Consistently longer dissociation times are observed for HC=O excitation than for H–CO excitation at the same EVL, especially at lower excitations. At higher excitation, the dissociation time seems to converge. As shown in Figure S4, the excitation is mode selective, but the energy redistribution along the H–C=O axis is rapid. This is partially a consequence of the classical nuclear dynamics in Car-Parrinello molecular dynamics (CPMD). The dissociation timescale then simply correlates with the energy uptake, as the ν_3 mode is ~ 700 cm^{-1} lower in energy than the ν_2 mode.

2.4. Mechanism of $[H_2–HCO]^+$ dissociation

The dissociation always proceeds via the same mechanism, shown in Figure 6. In the initial state, the H_2 monomer vibrates along the H–H bond, and pulses towards and away from the

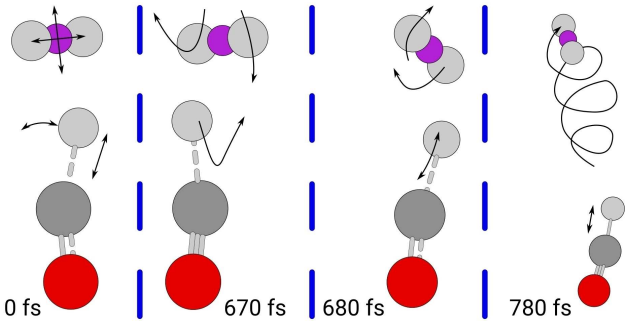

Figure 6. Snapshots in $[H_2–HCO]^+$ dissociation from a PBE0-D2 calculation with EVL = 2.2. Oxygen (red), carbon (dark gray), hydrogen (light gray) and center-of-mass of H_2 (pink).

HCO unit. The H–C bond is also vibrating, coupled to a sideways swing. When the H–C bond happens to pulse just as the H_2 moiety is approaching, it can effectively dampen the center-of-mass movement of the H_2 unit (see panel at 670 fs), and if it is excited enough, it can impart enough angular momentum to the other H-atom on the next swing (panel at 680 fs), so that the complex dissociates.

Occasionally, if the impulse provided by the H–C bond is not large enough, the $[H_2–HCO]^+$ complex may rearrange to the $[H_2<HCO]^+$ conformation. This conformer is stable enough to obtain a power spectrum, shown in Figure 7. The left panel of Figure 7 shows the shift and significantly higher intensity of the H_2···HCO mode in the out-of-plane isomer (red) compared to the global minimum (blue). Similarly, the H–CO vibration shifts from below 2800 cm^{-1} to above 3100 cm^{-1}, which is in a good agreement with the reported frequency of the H–CO mode in the HCO^+ ion[21] (yellow). This large shift in the two experimentally observed vibrational frequencies of the $[H_2–HCO]^+$ complex upon conformational change may also contribute to the observed line broadening.[10] In several non-dissociative cases, the complex remained in the out-of-plane conformation for up to 25% of the simulated time.

2.5. Dynamics of vibrationally excited $[D_2–DCO]^+$

The power spectrum of the deuterated complex is shown in Figure 8. By substituting all protium atoms with deuterium, the

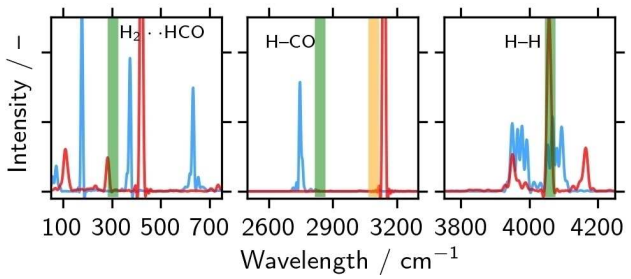

Figure 7. Normalised power spectra of $[H_2–HCO]^+$ (blue) and $[H_2<HCO]^+$ (red) calculated with PBE0-D2, compared to experimental data for $[H_2–HCO]^+$ (green)[10] and HCO^+ (yellow).[21]

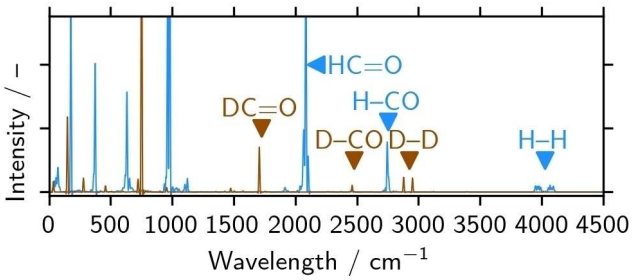

Figure 8. Normalised power spectra calculated with PBE0-D2 for $[H_2–HCO]^+$ (blue) and

vibrational modes shift to lower wavelengths, while the classical binding energy of the complex remains the same. This corresponds to a further lowering of the overall energy uptake at EVL = 1.0, by ~ 5 kJ/mol. However, this is still above the overall binding energy obtained with high-accuracy methods (cf. Table 1).

The results for the dissociation of the $[D_2–DCO]^+$ complex following a vibrational excitation, obtained with PBE0-D2, are shown in Figure 9 as brown symbols in addition to the protium

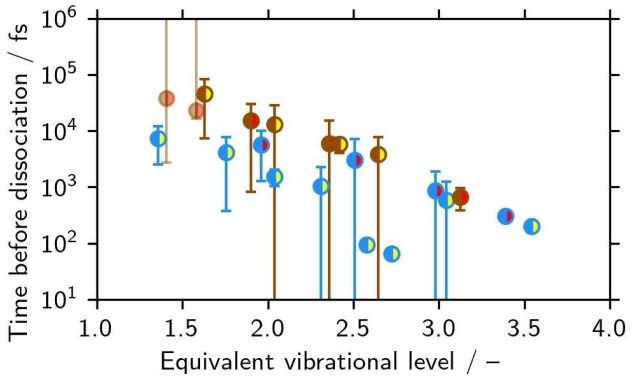

Figure 9. Time before dissociation for vibrationally excited $[H_2–HCO]^+$ (blue) and $[D_2–DCO]^+$ (brown). Results obtained with PBE0-D2 for C–H excitation (yellow shading) and C=O excitation (red shading). Error bars correspond to 3 standard errors ($3\times\sigma/\sqrt{4}$). In the two lowest-excitation cases (shaded), dissociation occurred within 100 ps only in 5 out of 8 cases.

data (blue). The results in HC=O excitation (red shading) are consistent with the protium data, with datapoints well within the 3-σ error bars. For the H–CO bond excitation (yellow shading), the dissociation in the deuterated complex is consistently slower than for the protium isotopologue, comparable in magnitude to the difference between ν_2 and ν_3 excitation.

2.6. Comparison with normal-mode excitation

A comparison of the available dissociation times of the protium and deuterium isotopologues of the complex is shown in Table 6. At the second vibrational level, the normal mode

Table 6. Dissociation times for the $[H_2–HCO]^+$ and $[D_2–DCO]^+$ complexes with excitations of various modes, to the first and second vibrationally excited state, with excitation using the external field or normal mode excitation. Results for external field excitation at integer excitations interpolated from data shown in Figs. 5 and 9.

Mode	Level	ZPE	Dissociation time / ps	
			External field	Normal mode
H—H	1.0	√	–	7
H—CO	1.0	√	–	26
HC═O	1.0	√	–	30
H—H	1.0	×	–	> 200
H—H	2.0	×	–	97
H—CO	1.0	×	–	41
H—CO	2.0	×	2 ± 1	9
HC═O	1.0	×	–	> 150
HC═O	2.0	×	5 ± 1	5
D—D	1.0	√	–	> 150
D—CO	1.0	√	–	> 200
DC═O	1.0	√	–	26
D—CO	1.0	×	–	79
D—CO	2.0	×	16 ± 5	11
DC═O	1.0	×	–	> 200
DC═O	2.0	×	8 ± 4	14

excitation shows an order-of-magnitude or better agreement with the excitation using external fields, further validating the external field excitation method.

The results confirm that the HC═O (ν_3) mode is less efficient at dissociating the complex than the H-CO (ν_2) mode. This can be attributed due to both poorer coupling of the ν_3 mode with the H_2···HCO (ν_4) intermonomer mode, as well as the fact that the dissociation barrier is overpredicted in the PBE0-D2 PES and can only be overcome once ZPE effects are considered. The deuterated results are in line with Figure 9. For the ν_2 mode at the first excited level the slowdown is significant (41→ 79 ps), while at the second excited level it is within the statistical uncertainty of the method. The normal mode excitation data at the first vibrational level for the $[H_2–HCO]^+$ confirms that excitation of the H–H mode does not cause a rapid dissociation until at least a second excited level is reached.

The H–H mode data in general, and the ZPE-corrected result in particular are doubtful, given the issues with the PBE0-D2 potential highlighted in the discussion of vibrational frequencies above. The effect of ZPE on the first excited state of ν_2 is also confusing: while in the protium complex it accelerates the dissociation, in the deuterated complex it helps redistribute the energy away from the intermonomer mode. In general, it is unclear whether it is always sensible to add the ZPE momenta to an otherwise classical MD.[22] In the current case, it seems to confound the inaccuracy in the H–H dynamics of the PBE0-D2 potential even further, and cannot be recommended.

2.7. Nuclear quantum effects

As the nuclear quantum effects may play a significant role in the dynamics of any system involving hydrogen atoms, we have attempted to estimate the error due to the classical representation of the nuclei in the CPMD calculations by applying the AICMD method to a selected case: $[D_2–DCO]^+$ excited to EVL = 2.36 using the ν_3 mode (HC═O). The same excited geometries as in the CPMD calculations are used as the starting point, without adding ZPE to the system. The calculations are extremely time demanding, with the computational cost scaling linearly with the Trotter dimension.

The CPMD dynamics with PBE0-D2 for the above case predict dissociation at 5.9 ps (σ = 3.1 ps, n = 4). With AICMD, applied with the same DFA and a Trotter dimension of 8, the dissociation timescale is 4.5 ps (σ = 1.9 ps, n = 5). This corresponds to a P-value of 0.43. The dissociation timescale does not significantly decrease with Trotter dimension set to 24.

The above results show that both CPMD and AICMD data are within the statistical error of the dataset. We are confident that most of the inaccuracy in the presented CPMD dissociation timescales is due to the overprediction of binding energies in the applied DFA, as opposed to the neglect of nuclear tunneling.

3. Conclusions

In the current work, we present an updated method of incorporating a periodic, time-dependent external field into Car-Parrinello calculations. We have applied this method to study the vibrational excitation and dissociation of the $[H_2–HCO]^+$ and $[D_2–DCO]^+$ systems. We have shown that the excitation is mode-selective and tunable, and that the dynamics of the system following an excitation are well-behaved.

The potential energy surface of the $[H_2–HCO]^+$ dimer has been investigated using a range of density functional and wavefunction methods, and compared to previously published data. The PBE0-D2 and to a lesser extent the PBE–D2 methods are both able to qualitatively model the main features of the $[H_2–HCO]^+$ system. Quantitatively, both DFT methods significantly overbind the complex at each minimum when compared to the highly-accurate MP2/CBS + δ(T) calculations. This translates to a potential slowdown in the PBE0-D2–based kinetics by a factor of 10^{-4} for H_2 internal rotation and 10^{-6} for a complete dissociation at 80 K. However, this will have impact only on the dissociation timescales themselves as opposed to the overall behaviour of the system. The potential surfaces around the stationary points obtained with the wavefunction methods are in agreement with the literature data of Bieske et al.,[10] confirming the presence of an out-of-plane $[H_2 < HCO]^+$ minimum.

The raw power spectra obtained directly from Car-Parrinello molecular dynamics trajectories, without correction for orbital inertia effects, are in a good agreement with the experimental infrared data of Bieske et al.[10] when PBE0-D2 is used. As expected, the anharmonic data from CPMD calculations is in a better agreement with experiment than the harmonic frequencies. However, correcting for the effect of increased electronic mass worsens the agreement in the ν_1 and ν_2 modes. This

disagreement at higher frequencies is attributed to the shape of the PBE0-D2 potential.

The dynamics of vibrationally excited $[H_2–HCO]^+$ and its deuterated analogue were investigated, by exciting the H–CO and HC=O stretching modes (ν_2 and ν_3) using external fields. The isotope effect in the dissociation of the complex is comparably weak, playing a significant role only when the H–CO mode is excited directly. For both H–CO and HC=O excitation, a significant energy transfer along the H–C=O axis is observed, while no such energy transfer is observed for H–H excitation in the dimer. The times before dissociation obtained from our calculations are consistent with the experimental observation of Bieske et al.:[10] an excitation to the first vibrationally-excited level of both H–CO and HC=O modes imparts enough kinetic energy to the system for a successful dissociation on a picosecond timescale. The dynamical timescales presented in the current work are overpredicted. The contribution to the overprediction due to the neglect of nuclear tunneling, roughly estimated at around ~ 25%, is overshadowed by the much more significant overprediction of the dissociation barriers when the chosen density functionals are compared to wavefunction theory, resulting in a slowdown factor of 10^{-6} at 80 K from barrier height considerations.

Finally, in addition to a complete dissociation of the complex, the observed broadening of the infrared spectrum[10] is likely also caused by an isomerisation forming the out-of-plane $[H_2<HCO]^+$ conformer with an infrared spectrum similar to uncomplexed HCO^+.

Supporting information summary

The supporting information contains: 1) the full computational details, 2) figure of all stationary points on the $[H_2–HCO]^+$ PES discussed in the current work, 3) description of the implementation of time-dependent external field in the CPMD program, 4) description of the tuning of the vibrational excitation using external fields, and 5) description of the excitation of $[H_2–HCO]^+$ using external fields.

Acknowledgements

This work was partially carried out on the Leibniz Universität Hannover compute cluster, which is funded by the Leibniz Universität Hannover, the Lower Saxony Ministry of Science and Culture (MWK) and the German Research Association (DFG).

Conflict of Interest

The authors declare no conflict of interest.

Keywords: Car-Parrinello · formyl cation · hydrogen complex · Molecular dynamics · non-covalent interactions

[1] V. Wakelam, I. W. Smith, E. Herbst, J. Troe, W. Geppert, H. Linnartz, K. Öberg, E. Roueff, M. Agúndez, P. Pernot, H. M. Cuppen, J. C. Loison, D. Talbi, *Space Sci. Rev.* **2010**, *156*, 13–72.
[2] S. Weinreb, A. H. Barrett, M. L. Meeks, J. C. Henry, *Nature* **1963**, *200*, 829–831.
[3] E. Herbst, W. Klemperer, *Astrophys. J.* **1974**, *188*, 255–256.
[4] W. Klemperer, V. Vaida, *Proc. Natl. Acad. Sci.* **2006**, *103*, 10584–10588.
[5] M. Yan, A. Dalgarno, W. Klemperer, A. E. S. Miller, *Mon. Not. R. Astron. Soc.* **2000**, *313*, L17–L18.
[6] D. Bates, E. Herbst, in *Rate Coefficients Astrochem.* (Eds.: T. Millar, D. Williams), Springer, **1988**, pp. 17–40.
[7] F. C. Fehsenfeld, D. B. Dunkin, E. E. Ferguson, *Astrophys. J.* **1974**, *188*, 43–44.
[8] K. Hiraoka, P. Kebarle, *J. Chem. Phys.* **1975**, *63*, 1688–1690.
[9] I. Frank, *ChemistrySelect* **2019**, *4*, 868–872.
[10] E. J. Bieske, S. A. Nizkorodov, F. R. Bennett, J. P. Maier, *J. Chem. Phys.* **1995**, *102*, 5152–5164.
[11] R. V. Olkhov, S. A. Nizkorodov, O. Dopfer, *J. Chem. Phys.* **1997**, *107*, 8229.
[12] H. Massó, L. Wiesenfeld, *J. Chem. Phys.* **2014**, *141*, 184301.
[13] B. Yang, N. Balakrishnan, P. Zhang, X. Wang, J. M. Bowman, R. C. Forrey, P. C. Stancil, *J. Chem. Phys.* **2016**, *145*, 034308.
[14] R. Liu, H. Xiong, M. Yang, *J. Chem. Phys.* **2012**, *137*, 174113.
[15] N. Mardirossian, M. Head-Gordon, *J. Chem. Phys.* **2016**, *144*, 214110.
[16] M. Brehm, B. Kirchner, *J. Chem. Inf. Model.* **2011**, *51*, 2007–2023.
[17] S. W. Ong, E. S. Tok, H. C. Kang, *Phys. Chem. Chem. Phys.* **2010**, *12*, 14960–14966.
[18] G. D. Dickenson, M. L. Niu, E. J. Salumbides, J. Komasa, K. S. Eikema, K. Pachucki, W. Ubachs, *Phys. Rev. Lett.* **2013**, *110*, 1–5.
[19] P. Luigi, M. Bernasconi, M. Parrinello, *Chem. Phys. Lett.* **1997**, *277*, 487–482.
[20] M. Thomas, M. Brehm, R. Fligg, P. Vöhringer, B. Kirchner, *Phys. Chem. Chem. Phys.* **2013**, *15*, 6608–6622.
[21] C. S. Gudeman, M. H. Begemann, J. Pfaff, R. J. Saykally, *Phys. Rev. Lett.* **1983**, *50*, 727–731.
[22] J. Ludwig, D. G. Vlachos, *Mol. Simul.* **2004**, *30*, 765–771.

Submitted: June 17, 2019
Accepted: August 23, 2019